



A screening model for quantifying PFAS leaching in the vadose zone and mass discharge to groundwater

Bo Guo ^{a,*}, Jicai Zeng ^a, Mark L. Brusseau ^{a,b}, Yonggen Zhang ^c

^a Department of Hydrology and Atmospheric Sciences, University of Arizona, United States Of America

^b Department of Environmental Science, University of Arizona, United States Of America

^c School of Earth System Sciences, Tianjin University, United States Of America

ARTICLE INFO

Keywords:

Per- and polyfluoroalkyl substances (PFAS)
Leaching
Interfacial adsorption
Analytical solution
Rate-limited adsorption
Unsaturated zone

ABSTRACT

A growing body of site investigations have demonstrated that vadose zones serve as significant long-term sources of PFAS to groundwater. Quantifying PFAS leaching in the vadose zone and mass discharge to groundwater is therefore critical for characterizing, managing, and mitigating long-term contamination risks. Mathematical models representing the PFAS-specific transport and retention processes, including surfactant-induced flow, and rate-limited, nonlinear adsorption at solid–water and air–water interfaces, have been recently developed. While these advanced models provide fundamental insights into the primary processes controlling the long-term retention of PFAS, they are less suitable for screening-type applications due to significant computational cost and the requirement for detailed input parameters. To address this knowledge gap, we develop a simplified model by assuming steady-state infiltration and linear solid-phase and air–water interfacial adsorption; a two-domain model is used to represent kinetic solid-phase adsorption. We derive novel analytical solutions for the simplified model allowing for arbitrary initial conditions. The newly derived analytical solutions are then validated by application to miscible-displacement experiments under a wide range of conditions and by comparisons to a state-of-the-art comprehensive model under both experimental and field conditions applicable to PFAS-contamination sites. Overall, the simplified analytical model provides an efficient and accurate screening-type tool for quantifying long-term PFAS leaching in the vadose zone.

1. Introduction

Per- and polyfluoroalkyl substances (PFAS) have become emerging contaminants of critical concern. Large-scale manufacturing and wide use of PFAS since the 1940s have led to their ubiquitous presence in the environment including surface water, soils, sediments, and groundwater. A growing body of site investigations have established that vadose zones are significant PFAS reservoirs that pose long-term threats for contaminating groundwater even several decades after the contamination events were stopped (Xiao et al., 2015; Weber et al., 2017; Dauchy et al., 2019; Høisæter et al., 2019; Anderson et al., 2019; Brusseau et al., 2020; Adamson et al., 2020; Cáñez et al., 2021).

Most PFAS are surfactants with unique interfacial properties that distinguish their transport behaviors from that of traditional non-surfactant contaminants. Laboratory measurements and analysis of surface tension data (Brusseau, 2018, 2019; Silva et al., 2019, 2021; Schaefer et al., 2019a; Costanza et al., 2019, 2020; Brusseau and Van Glubt, 2021) and miscible-displacement experiments under water-unsaturated conditions (Lyu et al., 2018; Brusseau et al., 2019b, 2021;

Lyu et al., 2020; Li et al., 2021) have demonstrated that PFAS tend to accumulate at air–water interfaces in soils, which can greatly increase retention in the vadose zone (e.g., Brusseau, 2018; Guo et al., 2020). Adsorption at the solid–water interfaces resulting from hydrophobic and electrostatic interactions also enhances the retention of PFAS in soils (e.g., Higgins and Luthy, 2006; Barzen-Hanson et al., 2017; Xiao et al., 2019; Mejia-Avenidaño et al., 2020; Wang et al., 2021). Additional processes including volatilization, transformation of precursors, and uptake by biota can add further complexities to the retention of some PFAS in the vadose zone (e.g., Sima and Jaffé, 2020; Sharifan et al., 2021).

Mathematical models representing the complex retention and leaching processes of PFAS in soils are critically needed for understanding long-term risks of vadose-zone PFAS as a source of contamination to groundwater. Guo et al. (2020) reported a new mathematical model that accounts for a set of unique transport behaviors of PFAS in the vadose zone, including nonlinear and rate-limited adsorption at solid–water and air–water interfaces in the presence of transient

* Corresponding author.

E-mail address: boguo@arizona.edu (B. Guo).

<https://doi.org/10.1016/j.advwatres.2021.104102>

Received 27 July 2021; Received in revised form 24 November 2021; Accepted 12 December 2021

Available online 3 January 2022

0309-1708/© 2022 Elsevier Ltd. All rights reserved.

variably saturated flow and surfactant-induced flow. The mathematical model has been validated by application to water-unsaturated miscible-displacement column experiments under a wide range of conditions (El Ouni et al., 2021; Brusseau et al., 2021; Zeng et al., 2021) and applied to simulate long-term PFAS leaching at a model fire training area site (Guo et al., 2020; Zeng et al., 2021). The simulated strong retention of PFAS in the shallow vadose zone is consistent with many prior field observations (e.g., Anderson et al., 2019; Dauchy et al., 2019; Høisæter et al., 2019; Brusseau et al., 2020). Shortly thereafter, a model similar to that of Guo et al. (2020) was independently reported by Silva et al. (2020), rate-limited adsorption was not considered, where example simulations were presented in one- and two-dimensions. More recently, Zeng and Guo (2021) extended the model formulations of Guo et al. (2020) to three dimensions and examined the impact of surfactant-induced flow and preferential flow on long-term PFAS leaching in heterogeneous vadose zones.

While the comprehensive models discussed above provide fundamental insights into the primary processes controlling the long-term retention and leaching of PFAS in the vadose zone, their complexity and the associated significant computational cost make them less suitable for practical screening-type application at field contamination sites, such as for developing initial strategies for characterizing, managing, and mitigating PFAS contamination risks based on limited site information. Screening-type analysis usually employs much simpler analytical or semi-analytical models that are computationally efficient and do not need detailed information for the input parameters and site conditions. Such simple models have been previously demonstrated as useful screening tools for guiding remediation strategies and determining regulatory standards for non-PFAS contaminants. Examples include the EPA spreadsheet model for subsurface vapor intrusion (US-EPA, 2017) and REMChlor-MD for modeling long-term matrix diffusion of chlorinated solvent in aquifers (Falta et al., 2018). However, similar simple models for quantifying PFAS leaching in the vadose zone and mass discharge to groundwater are to date not available.

In the present work, we address this knowledge gap by developing a simplified model for PFAS retention and leaching in the vadose zone that allows for analytical solutions. Specifically, our model formulation assumes steady-state infiltration and simplifies the transport processes by linearizing the nonlinear terms for adsorption at the solid–water and air–water interfaces. Additionally, rate-limited adsorption at the solid–water interfaces is represented by a two-domain kinetic model. New analytical solutions derived for the simplified model are validated by application to miscible-displacement experiments for multiple PFAS under a wide range of conditions as well as via comparisons to simulations produced with a comprehensive numerical model under both experimental and field conditions. To the best of our knowledge, the analytical solutions presented here are the first for solute transport that account for the two-domain solid-phase kinetic adsorption and air–water interfacial adsorption. Finally, we present a workflow to demonstrate the application of the simplified models for analyzing long-term PFAS leaching in the vadose zone.

2. Mathematical model and simplifications

We present the mathematical model from simplifying both the variably saturated flow and PFAS transport processes represented in the model formulations of Guo et al. (2020).

2.1. Water flow

We consider water flow driven by steady-state infiltration in the vertical dimension of a homogeneous vadose zone. Water in the vadose zone is assumed unsaturated with a spatially uniform saturation, i.e., $\frac{\partial h}{\partial z} = 0$ where h is the water pressure head, and the unsaturated

water flow q (cm/s) is driven only by gravity. Assuming that z is positive downward, from Darcy's law $q = -K \frac{\partial}{\partial z} (h - z)$, we obtain

$$q = K, \quad (1)$$

where K is the unsaturated hydraulic conductivity (cm/s), which can be approximated as an empirical function of the volumetric water content, θ (-). Here we present the widely used empirical function proposed by Mualem (1976) and van Genuchten (1980) as an example

$$K(\theta) = K_s S_{w,e}^\lambda \left[1 - \left(1 - S_{w,e}^{1/m} \right)^m \right]^2, \quad (2)$$

where K_s is the saturated conductivity (cm/s). $S_{w,e} = \frac{\theta - \theta_r}{\theta_s - \theta_r}$ is the effective water saturation (-), where θ_r and θ_s are the residual and saturated water contents (cm³/cm³), respectively. λ and m are empirical parameters. λ can vary for different soil media, though it is often set to 0.5 for simplicity. m is related to the pore-size distribution of the soil media and can be determined by fitting the soil water characteristic function of van Genuchten (1980) to measured datasets. We note that alternative models for K , such as the equations proposed by Kosugi (1999), may also be employed. The Kosugi model was shown to match better the measured unsaturated water conductivity than Eq. (2) for some soil media.

2.2. Transport of PFAS

Transport of PFAS in the vertical dimension of a vadose zone may be described by an advection–dispersion equation coupled with solid-phase and air–water interfacial adsorption terms (e.g., Brusseau, 2020; Guo et al., 2020)

$$\frac{\partial(\theta C)}{\partial t} + \rho_b \frac{\partial C_s}{\partial t} + \frac{\partial C_{aw}}{\partial t} + \frac{\partial}{\partial z} (\theta v C) - \frac{\partial}{\partial z} \left(\theta D \frac{\partial C}{\partial z} \right) = 0, \quad (3)$$

where C is the aqueous concentration (μmol/cm³). C_{aw} is the adsorption at air–water interfaces (μmol/cm³). C_s is the solid-phase adsorption (μmol/cm³). $v = q/\theta$ is the interstitial porewater velocity (cm/s). $D = \alpha_L v + \tau D_0$ is the dispersion coefficient (cm²/s), where α_L is the longitudinal dispersivity (cm) and D_0 is the molecular diffusion coefficient in free water. The tortuosity τ can be approximated as $\tau = \frac{\theta^{7/3}}{\theta_s^2}$ (Millington and Quirk, 1961).

The solid-phase adsorption C_s can be modeled by the nonlinear Freundlich isotherm (Higgins and Luthy, 2006; Wei et al., 2017; Brusseau et al., 2019a; Van Glubt et al., 2020). The fitted exponent parameter in the Freundlich isotherm was reported to range from 0.75 to 1.1 for multiple PFAS in a wide range of soils and sediments (Higgins and Luthy, 2006; Guelfo and Higgins, 2013; Van Glubt et al., 2020). A recent study showed that the fitted exponent parameter ranged from 0.64 to 1.27 (median: 0.82 and mean: 0.85) for PFOS in 114 tropical and temperate soils (Umeh et al., 2021). Because the present study focuses on formulating a simplified model for which analytical solutions can be derived, we assume that the solid-phase adsorption can be approximated by a linear isotherm. Kinetics associated with solid-phase adsorption were shown to be present in both batch and miscible-displacement experiments (Brusseau et al., 2019a; Guelfo et al., 2020; Schaefer et al., 2021; Zhou et al., 2021). Guelfo et al. (2020) and Schaefer et al. (2021) suggested that kinetic solid-phase adsorption is only present in real soils with organic carbon or clay content greater than 0. We use a two-domain model to represent kinetic solid-phase adsorption, i.e., $C_s = C_{s,1} + C_{s,2}$, where $C_{s,1}$ is the adsorbed concentration in the “instantaneous” sorption domain and $C_{s,2}$ is the adsorbed concentration in the kinetic sorption domain.

$$C_{s,1} = F_s K_d C, \quad (4)$$

$$\frac{dC_{s,2}}{dt} = \alpha_s \left[(1 - F_s) K_d C - C_{s,2} \right], \quad (5)$$

where K_d is the solid-phase adsorption coefficient (cm^3/g), F_s is the fraction of sorbent for which sorption is instantaneous, α_s is the first-order rate constant for kinetic sorption. Miscible-displacement experiments using soil-packed columns have demonstrated that the kinetics associated with air–water interfacial adsorption is minimal under steady-state flow conditions (Brusseau, 2020; Brusseau et al., 2021). We thus assume equilibrium air–water interfacial adsorption. The adsorption at air–water interfaces C_{aw} in Eq. (3) is the product of the surface excess Γ ($\mu\text{mol}/\text{cm}^2$) and the air–water interfacial area A_{aw} (cm^2/cm^3)

$$C_{aw} = \Gamma A_{aw}, \quad (6)$$

where the surface excess Γ is a function of the aqueous concentration, $\Gamma = K_{aw} C$. K_{aw} (cm^3/cm^2) is the air–water interfacial adsorption coefficient, which under the ideal dilute solution assumption (i.e., below the critical micelle concentration) can be computed based on the Gibbs equation (e.g., Kissa, 2001; Rosen and Kunjappu, 2012)

$$K_{aw} = \frac{\Gamma}{C} = -\frac{1}{\chi R_g T C} \left(\frac{\partial \sigma}{\partial \ln C} \right)_T, \quad (7)$$

where R_g is the universal gas constant ($\text{J}/\text{K}/\text{mol}$) and T is temperature (K). χ is a coefficient that equals to 1 for a nonionic PFAS or an ionic PFAS in the presence of a swamping amount of electrolyte, or 2 for an ionic PFAS with no swamping electrolyte. Surface tension σ for a solution with a single PFAS can be modeled by the Szyszkowski equation (e.g., Chang and Franses, 1995; Adamson and Gast, 1997)

$$\sigma = \sigma_0 \left[1 - b \ln \left(1 + \frac{C}{a} \right) \right], \quad (8)$$

where σ_0 is the surface tension of the aqueous solution with no dissolved PFAS (dyn/cm), and a ($\mu\text{mol}/\text{cm}^3$) and b (–) are fitting parameters to experimental data. Substituting Eq. (8) into Eq. (7) yields

$$K_{aw} = \frac{1}{\chi R_g T} \frac{\sigma_0 b}{a + C}, \quad (9)$$

Substituting Eqs. (4)–(6) to Eq. (3), we obtain a linear advection–dispersion equation (Eq. (10)) coupled with a two-domain kinetic solid-phase adsorption model (Eq. (5)).

$$\beta R \frac{\partial C}{\partial t} + \frac{\rho_b \alpha_s}{\theta} [(1 - F_s) K_d C - C_{s,2}] + \frac{\partial}{\partial z} (vC) - \frac{\partial}{\partial z} \left(D \frac{\partial C}{\partial z} \right) = 0, \quad (10)$$

where the retardation factor $R = 1 + R_s + R_{aw}$ and $\beta = (1 + F_s R_s + R_{aw}) / R$. $R_s = \rho_b K_d / \theta$ and $R_{aw} = K_{aw} A_{aw} / \theta$ represent the retardation from solid-phase and air–water interfacial adsorption, respectively.

For PFAS migration in the vadose zone, we consider the following initial and boundary conditions for Eqs. (10) and (5) assuming that PFAS are released to a semi-infinite vadose zone at a constant concentration C_0 for the time period $0 < t < t_0$.

$$C(z, 0) = C_i(z), \quad (11)$$

$$C_{s,2}(z, 0) = C_{s,2,i}(z), \quad (12)$$

$$\left(-D \frac{\partial C}{\partial z} + vC \right) \Big|_{z=0} = \begin{cases} vC_0 & 0 < t \leq t_0 \\ 0 & t > t_0, \end{cases} \quad (13)$$

$$\frac{\partial C}{\partial z} \Big|_{z=\infty} = 0. \quad (14)$$

where $C_i(z)$ and $C_{s,2,i}(z)$ are initial concentrations in the aqueous phase and in the kinetic sorption domain, respectively. Assuming equilibrium initially, $C_{s,2,i} = (1 - F_s) K_d C_i$.

We note that the air–water interfacial area (A_{aw}) in Eq. (6) in soils is comprised of two types including capillary interfaces associated with menisci between bulk air and water and film-related interfaces associated with wetting films surrounding grain surfaces, both of which are relevant for PFAS transport as demonstrated by prior miscible-displacement experiments (Lyu et al., 2018, 2020; Brusseau et al., 2019b, 2021; Li et al., 2021; Brusseau and Guo, 2021). The combination of the two, i.e., the total air–water interfacial area, is considered

in the present study. The total A_{aw} usually increases as S_w decreases. We approximate A_{aw} as a second degree polynomial function of water saturation S_w

$$A_{aw} = x_2 S_w^2 + x_1 S_w + x_0, \quad (15)$$

where x_2 , x_1 , and x_0 are parameters that can be determined by fitting to air–water interfacial area data measured by aqueous interfacial tracer methods. When measured A_{aw} based on aqueous interfacial tracer methods are not available, A_{aw} may be estimated using the thermodynamic-based approach (Leverett, 1941; Morrow, 1970; Bradford and Leij, 1997). The thermodynamic-based method is described in more detail in Section 5 and employed for the soil media therein.

3. Analytical solutions

We derive new analytical solutions for Eqs. (5) and (10) subject to the initial and boundary conditions of Eqs. (11)–(14) using the Laplace transform. Similar derivation procedures were reported in the literature for solute transport in the presence of kinetic solid-phase adsorption with no air–water interfacial adsorption (Lindstrom and Narasimham, 1973; van Genuchten and Wagenet, 1989; Toride et al., 1993), we therefore only present the final form of the analytical solutions with the detailed and rather tedious derivation steps omitted. To the best of our knowledge, the analytical solution reported here is the first that accounts for the two-domain solid-phase kinetic adsorption and air–water interfacial adsorption.

For convenience, we define the following dimensionless variables and parameters $T = vt/L$, $T_0 = v t_0/L$, $Z = z/L$, $P = vL/D$, $\omega_s = \alpha_s (1 - \beta_s) (1 + R_s) L/v$, where L is an arbitrary distance from the land surface, which is taken as the depth of the vadose zone in the present study, and $\beta_s = (1 + F_s R_s) / (1 + R_s)$. ω_s is often referred to as the Damköhler number, which represents the ratio between the characteristic time scales of transport (i.e., advection in the present study) and reaction (i.e., kinetic solid-phase adsorption in the present study).

Because Eqs. (5) and (10) and the boundary conditions are linear, the analytical solutions for the aqueous concentration $C(Z, T)$ and adsorbed concentration at the kinetic sorption domain $C_{s,2}(Z, T)$ can be considered as the sum of the solutions for the boundary value problem (BVP) and the initial value problem (IVP), i.e., $C(Z, T) = C^{BVP}(Z, T) + C^{IVP}(Z, T)$ and $C_{s,2}(Z, T) = C_{s,2}^{BVP}(Z, T) + C_{s,2}^{IVP}(Z, T)$. The solutions for the boundary value problem are

$$C^{BVP}(Z, T) = \begin{cases} C_0 A(Z, T), & 0 < T \leq T_0 \\ C_0 A(Z, T) - C_0 A(Z, T - T_0), & T > T_0 \end{cases} \quad (16)$$

$$C_{s,2}^{BVP}(Z, T) = \begin{cases} C_0 (1 - F_s) K_d B(Z, T), & 0 < T \leq T_0 \\ C_0 (1 - F_s) K_d B(Z, T) \\ - C_0 (1 - F_s) K_d B(Z, T - T_0), & T > T_0 \end{cases} \quad (17)$$

where

$$A(Z, T) = \int_0^T g(Z, \tau) J(a_1, b_1) d\tau, \quad (18)$$

$$B(Z, T) = \int_0^T g(Z, \tau) [1 - J(b_1, a_1)] d\tau, \quad (19)$$

$$J(a_1, b_1) = 1 - e^{-b_1} \int_0^{a_1} e^{-\lambda} I_0 \left[2\sqrt{b_1 \lambda} \right] d\lambda, \quad (20)$$

$$a_1 = \frac{\omega_s \tau}{\beta R}, \quad (21)$$

$$b_1 = \frac{\omega_s (T - \tau)}{(1 - \beta_s) (1 + R_s)}, \quad (22)$$

$$g(Z, \tau) = \left(\frac{P}{\pi \beta R \tau} \right)^{1/2} e^{\left[-\frac{P(\beta R Z - \tau)^2}{4\beta R \tau} \right]} - \frac{P}{2\beta R} e^{PZ} \times \text{erfc} \left[\left(\frac{P}{4\beta R \tau} \right)^{1/2} (\beta R Z + \tau) \right]. \quad (23)$$

In addition to the volume-averaged resident concentration $C(Z, T)$ (i.e., mass of solute per unit volume of fluid), the flux-averaged concentration (i.e., mass of solute per unit volume of fluid passing through a given cross-section) may also be of interest when simulating the breakthrough concentrations for miscible-displacement experiments (Kreft and Zuber, 1978; van Genuchten and Parker, 1984). For flux-averaged concentration, $g(Z, \tau)$ is given by

$$g(Z, \tau) = \frac{Z}{\tau} \left(\frac{P\beta R}{4\pi\tau} \right)^{1/2} e^{-\frac{P(\beta R Z - \tau)^2}{4\beta R\tau}} \quad (24)$$

The Goldstein's J function in Eq. (20) can be approximated in various ways as summarized by van Genuchten (1981). In the present study, we employ the approximation based on the modified Bessel function given by Lindstrom and Stone (1974).

The solutions for the initial value problem are

$$C^{IVP}(Z, T) = e^{-\frac{\omega_s T(1-F_s)R_s}{(1-\beta_s)(1+R_s)\beta R}} G(Z, T) + \frac{\omega_s}{(1-\beta_s)(1+R_s)} \times \int_0^T H(T, \tau)G(Z, \tau)d\tau, \quad (25)$$

where

$$G(Z, T) = \int_0^{+\infty} C_i(\xi) \left\{ \frac{e^{-\frac{P\beta R}{4T}(Z-\xi-T/\beta R)^2} + e^{-\xi P - \frac{P\beta R}{4T}(Z+\xi-T/\beta R)^2}}{2\sqrt{\frac{\pi T}{\beta R P}}} - \frac{P}{2} e^{PZ} \operatorname{erfc} \left(\frac{Z + \xi + T/\beta R}{2\sqrt{\frac{T}{\beta R P}}} \right) \right\} d\xi, \quad (26)$$

$$H(T, \tau) = \frac{R_s(1-F_s)}{\beta R} e^{-\frac{\omega_s(T-\tau)}{(1-\beta_s)(1+R_s)} - \frac{\omega_s\tau(1-F_s)R_s}{(1-\beta_s)(1+R_s)\beta R}} \left\{ I_0 \left[\frac{2\omega_s}{(1-\beta_s)(1+R_s)} \sqrt{\frac{R_s(1-F_s)(T-\tau)\tau}{\beta R}} \right] + \frac{\tau I_1 \left[\frac{2\omega_s}{(1-\beta_s)(1+R_s)} \sqrt{\frac{R_s(1-F_s)(T-\tau)\tau}{\beta R}} \right]}{\sqrt{R_s(1-F_s)(T-\tau)\tau/\beta R}} \right\}. \quad (27)$$

$$C_{s,2}^{IVP}(Z, T) = C_{s,2,i}(Z) e^{-\frac{\omega_s T}{(1-\beta_s)(1+R_s)}} + \frac{\omega_s}{(1-\beta_s)(1+R_s)} \times \int_0^T (1-F_s)K_d G(Z, \tau)H_{s,2}(T, \tau)d\tau, \quad (28)$$

where

$$H_{s,2}(T, \tau) = e^{-\frac{\omega_s(T-\tau)}{(1-\beta_s)(1+R_s)} - \frac{\omega_s\tau(1-F_s)R_s}{(1-\beta_s)(1+R_s)\beta R}} \left\{ I_0 \left[\frac{2\omega_s}{(1-\beta_s)(1+R_s)} \sqrt{\frac{R_s(1-F_s)(T-\tau)\tau}{\beta R}} \right] + \sqrt{\frac{R_s(1-F_s)(T-\tau)}{\beta R\tau}} \times I_1 \left[\frac{2\omega_s}{(1-\beta_s)(1+R_s)} \sqrt{\frac{R_s(1-F_s)(T-\tau)\tau}{\beta R}} \right] \right\}. \quad (29)$$

We make two comments on the analytical solutions presented above. (1) The analytical solutions can be greatly simplified when kinetic solid-phase adsorption is not considered. In that case, $F_s = 1$, $C_{s,2} = 0$, $J(a_1, b_1) = 1$, and $A(Z, T)$ can be integrated analytically. The analytical solution for this special case with no kinetic solid-phase adsorption is presented in Appendix. (2) The simplified model in

Section 2 is more general than the analytical solutions presented in Section 3 because the transport equation (Eq. (10)) can involve spatial heterogeneities. For example, the solid-phase adsorption coefficient K_d can be a depth-dependent function to reflect the change of sorption capacities along depth, e.g., decrease of organic carbon content along the soil profile. Additionally, the more general Freundlich nonlinear adsorption model can also be used for representing solid-phase adsorption. However, the presence of nonlinearities and heterogeneities would generally prevent the transport equation from being solved analytically.

4. Model validation and evaluation

We validate the simplified analytical model by simulating breakthrough curves measured in multiple miscible-displacement experiments reported in the literature and by conducting simulations of PFAS leaching in the vadose zone at a model fire training area site under field-relevant conditions. The analytical-based simulations are in both cases compared to numerical solutions of the full-process model of Guo et al. (2020).

4.1. Simulating miscible-displacement experiments

We simulate three sets of PFAS unsaturated miscible-displacement experiments reported in the literature. All of the experiments were conducted using columns packed with a commercially available natural quartz sand (UNIMIN Corp.) referred to as Accusand, which has a mean grain diameter of 0.35 mm and a total organic carbon content of 0.04%. Aggregated data for the air-water interfacial area under a wide range of water saturations for Accusand were summarized in Jiang et al. (2020). The air-water interfacial area measured by aqueous interfacial tracer methods was fitted to a second degree polynomial function of water saturation (Eq. (15); $x_2 = 548.54$, $x_1 = -1182.5$, $x_0 = 633.96$) by Guo et al. (2020), and is employed here for simulating the experiments.

The first set of experiments were conducted for PFOA at three different input concentrations (0.01, 0.1, and 1 mg/L), but only the arrival fronts of the breakthrough curves were measured (Lyu et al., 2018). The second set of experiments was conducted for PFOS at an input concentration of 0.1 mg/L (Brusseau et al., 2021). The third set of experiments was conducted for hexafluoropropylene oxide dimer acid (HFPO-DA, also known as GenX) at an input concentration of 10 mg/L (Yan et al., 2020). Full breakthrough curves were measured for both the second and third sets of experiments. The water saturation of the sand column was 0.68, 0.68, and 0.64 for the three sets of experiments, respectively.

All of the miscible-displacement experiments were conducted using a background electrolyte solution of 0.01 M NaCl solution. The surface tension of the NaCl solution with no PFAS is $\sigma_0 = 71.4$ dyn/cm. The Szyskowski parameters for the five PFAS in the NaCl solution are: PFBA ($a = 4702.6$ mg/L, $b = 0.19$), PFHxA ($a = 502.1$ mg/L, $b = 0.17$), PFOA ($a = 78.6$ mg/L, $b = 0.2$), PFOS ($a = 5$ mg/L, $b = 0.1$), GenX ($a = 109$ mg/L, $b = 0.1$). The hydraulic parameters of the sand were measured in the lab and were reported in Guo et al. (2020). The solid-phase adsorption parameters were determined from transport experiments conducted under water-saturated conditions. It is important to point out that all of the parameters are determined independently with no fitting or calibration, thus the model simulations are predictions of the experiments and comparisons between the simulations and measurements represent a direct validation test of the model.

The experimental data and the simulations from both the simplified analytical model and the full-process numerical model are presented in Fig. 1. The flux-averaged concentration at the outlet is used in the analytical solution. The results show that the predictions from both the analytical and numerical models agree well with the experimental data. The case that sees some deviation is PFOA with an input concentration of 0.1 mg/L in the first set of experiments. This may be caused by

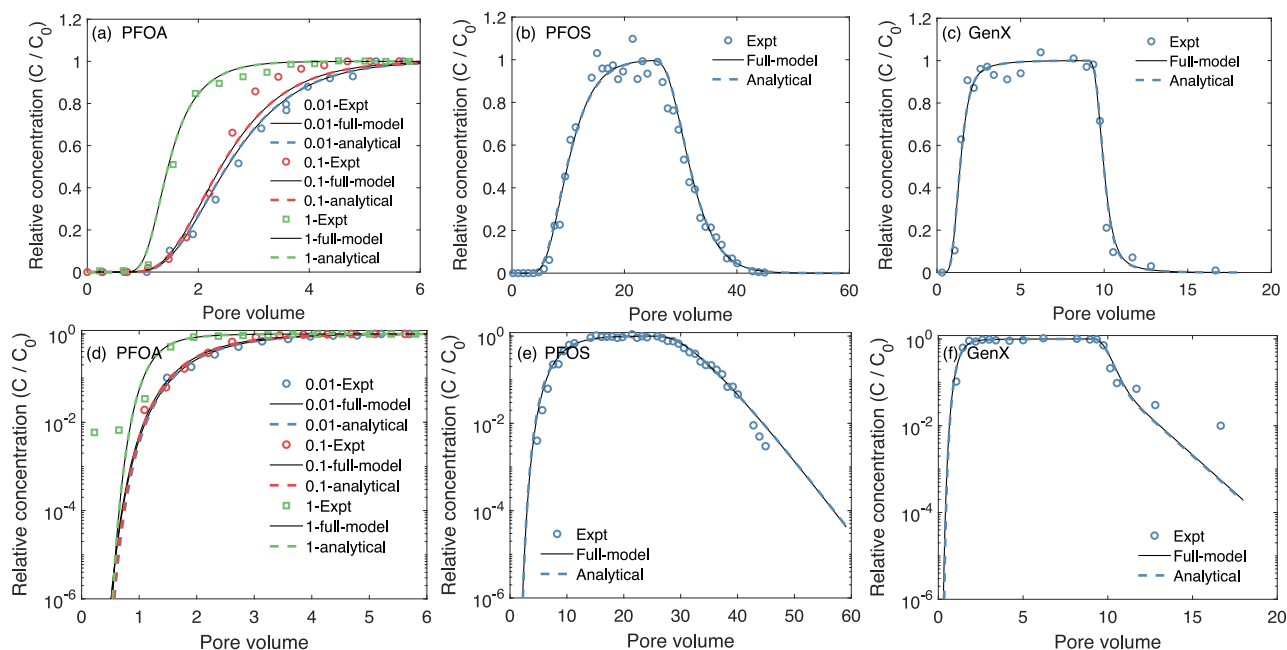


Fig. 1. Comparisons of the breakthrough curves simulated by the simplified analytical model (dashed lines) and full-process numerical model (solid lines), and measured (symbols) from the miscible-displacement experiments under water-unsaturated conditions. (a), (b), and (c) correspond to the three sets of miscible-displacement experiments described in Section 4.1, respectively. (d), (e), and (f) are the semi-log version of the plots.

variability in the kinetics of the solid-phase adsorption among the three columns in this set of experiments—the kinetic parameters were determined from one of the columns under saturated condition and then employed for all three columns. The comparisons in the semi-log plots (d–f) are generally consistent with those in the arithmetic plots (a–c). The low concentration data points at approximately 0.2 pore volume for PFOA (d) and 17 pore volumes for GenX (f) are near the detection limit of the analytical method and hence may not be accurate. Some deviation between the model simulations and the experimental data is observed for the two data points at approximately 12 and 13 pore volumes for GenX. This deviation indicates that there may be nonideal adsorption kinetics that are not captured by the two-domain kinetic sorption model employed in the simulations. According to the data and analysis presented in Brusseau et al. (2019a), this long tailing behavior observed for GenX is most likely caused by nonideal adsorption at the solid surfaces. We would like to point out that Guelfo et al. (2020)—using a similar sand but with a total organic carbon content of 0—concluded that the solid-phase adsorption is not rate limited under the conditions examined in their experiments.

It is interesting that the analytical solutions are almost identical to the numerical solutions from the full-process model for all of the experiments. This implies that the additional processes included in the full-process model have a minimal impact on PFAS transport under the specific conditions employed in the experiments, i.e., relatively low input concentrations. These observations are consistent with the results reported in Brusseau et al. (2021), which concluded that surfactant-induced flow and nonlinearity in air–water interfacial adsorption are insignificant under those miscible-displacement experimental conditions when the input concentration is sufficiently below the critical reference concentration (i.e., the concentration corresponding to 2.5% of reduction in surface tension). Given that the simulations are predictions with no parameter fitting, the excellent agreement with the experimental data and the full-process numerical model demonstrates the validity of the simplified analytical model for representing the transport processes of PFAS in water-unsaturated miscible-displacement experiments.

4.2. Simulating PFAS retention and leaching at a model AFFF-impacted fire training area site

We further evaluate the simplified analytical model by comparing it to the full-process numerical model for simulating long-term retention and leaching of PFAS in the vadose zone under field-relevant conditions. We consider a model aqueous film-forming foam (AFFF)-impacted fire training area site with a 30-year contamination period (PFAS are being released to the vadose zone due to regular fire training activities) and a 50-year post-contamination period (fire training activities are stopped and no additional PFAS are being released to the vadose zone). A 4-m deep vadose zone is assumed homogeneous and is composed of one of two porous media (Accusand and Vinton soil) for which extensive prior laboratory measurements are available. The detailed hydraulic and transport parameters for Accusand and Vinton soil were reported in Guo et al. (2020). We consider four representative PFAS including two short-chain compounds (PFPeA and PFHxS) and two long-chain compounds (PFOA and PFOS). As suggested by Guo et al. (2020) based on standard practices at fire training area sites, the fire training is assumed to occur every ten days with each training lasting for 30 mins leading to a total infiltration of 0.0458 cm of diluted AFFF solution per training session. PFAS composition in AFFF varies among different products and in different years (Houtz et al., 2013). Here we adopt the composition reported in Høisæter et al. (2019) for a commercial AFFF. With a 1:100 dilution, the concentrations for PFPeA, PFHxS, PFOA, and PFOS are 0.23, 7.1, 0.9, and 100 mg/L, respectively. The surface tension data for the PFAS measured in synthetic groundwater are used to determine the Szyskowski parameters, which are presented together with other PFAS in Section 5 (Table 2). Similar to the simulations reported in Guo et al. (2020), rainfall and evapotranspiration data measured at 30-min resolution from a site in Arizona (AZ) and a site in New Jersey (NJ) downloaded from the AmeriFlux database (URL: <https://ameriflux.lbl.gov/>) are used to represent semiarid and humid regions, respectively.

Both models consider a one-dimensional domain along the vertical dimension of the vadose zone. The numerical model employs a uniform grid ($\Delta z = 1$ cm). Free drainage (i.e., normal gradient of capillary pressure is zero) and zero dispersion (i.e., advective flux

Table 1

Parameters for the solid-phase adsorption of four PFAS (PFPeA, PFHxS, PFOA, and PFOS) in Accusand and Vinton soil. C_{rep} is the representative concentration at which the nonlinear Freundlich isotherm is linearized to a linear isotherm ($K_d = K_f C_{rep}^{N-1}$) for the simplified analytical model.

Soil media	PFAS	K_f (mg/kg)/(mg/L) ^N	N	C_{rep} mg/L	K_d cm ³ /g	F_s	α_s 1/h
Accusand	PFPeA	0.0211	0.87	0.005	0.0420	0.4	5.9
	PFHxS	0.0213	0.81	0.15	0.0305	0.1	3.1
	PFOA	0.1	0.87	0.016	0.1712	0.4	5.9
	PFOS	0.15	0.81	1	0.15	0.1	3.1
Vinton	PFPeA	0.122	0.87	0.005	0.2429	0.16	0.9
	PFHxS	0.156	0.77	0.15	0.2413	0.16	0.9
	PFOA	0.58	0.87	0.016	0.9929	0.16	0.9
	PFOS	1.11	0.77	1	1.11	0.16	0.9

only) are assumed at the bottom boundary. The full-process model accounts for surfactant-induced flow, rate-limited and nonlinear solid-phase adsorption, and rate-limited and nonlinear air–water interfacial adsorption (Guo et al., 2020). The coupled Richards' equation and nonlinear advection–dispersion equation are solved in a fully implicit numerical framework by Newton–Raphson iterations. Further details about the model setup and numerical algorithms for the full-process model can be found in Guo et al. (2020). For the simplified analytical model, we need to make three simplifications to represent the field conditions. (1) Since the analytical solution can only represent steady-state infiltration, we take the average annual net infiltration rate computed from the numerical simulations and convert it to steady-state infiltration. (2) We also need to compute the average PFAS infiltration and convert it to steady-state infiltration during the active-contamination period. (3) Finally, the nonlinear solid-phase adsorption and air–water interfacial adsorption both need to be linearized; the linear solid-phase adsorption coefficients $K_d = K_f C_{rep}^{N-1}$ are computed at representative concentration values (see Table 1), while the constant air–water interfacial adsorption coefficient K_{aw} is computed at $C = 0$ mg/L for simplicity.

Comparisons between the simulations from the simplified analytical model and the full-process numerical model are presented in Figs. 2 and 3. Despite the various assumptions employed by the analytical model, the simplified analytical model agrees well with the full-process numerical model for the simulated retention (i.e., mass remaining in the vadose zone) and cumulative mass discharge to groundwater (Fig. 2) as well as the time-dependent spatial profiles of PFAS concentrations in the vadose zone (Fig. 3). An exception is PFOS, where the simplified analytical model substantially underestimates the leaching compared to the full-process numerical model.

The underestimated leaching observed for PFOS may be attributed to two of the assumptions made in the simplified analytical model: (1) steady-state infiltration and (2) linear air–water interfacial adsorption. While transient variably saturated flow due to time-dependent rainfall infiltration does not substantially change water saturation at deeper locations in the vadose zone, it leads to significant changes in the water saturation near the land surface. The increases in water saturation during rainfall events destroy air–water interfaces and reduce air–water interfacial adsorption, which then leads to accelerated leaching of PFAS. This phenomenon has a more significant impact on the leaching of PFOS because it is more strongly retained in soils and stays in the shallow vadose zone for a longer period of time. A close inspection also reveals that the impact of transient infiltration has a greater impact during the active contamination period because transient infiltration dynamically redistributes the released PFAS near the land surface. This is not accounted for in the simplified analytical model so its simulated concentration profiles deviate from those simulated by the full-process model during the active contamination period ($t \leq 30$ years), especially near the land surface. Concomitantly, the release concentration of PFOS (100 mg/L) is the highest among the four PFAS, which leads

to stronger nonlinear air–water interfacial adsorption. Therefore, using the maximum $K_{aw} = 0.048$ cm³/cm² (i.e., $C = 0$ mg/L) in the analytical solution underestimates leaching of PFOS in the vadose zone.

To further illustrate the influence of the two assumptions discussed above and to explore ways to improve the prediction of the simplified analytical model, we conduct two sets of additional simulations for PFOS using the simplified analytical model. The first set of simulations uses $K_{aw} = 0.038$ cm³/cm² corresponding to a representative aqueous concentration in the vadose zone ($C_{rep} = 1$ mg/L). The representative concentration is estimated from the original simulated plume (i.e., assuming maximum K_{aw}). Note that the representative aqueous concentration in the vadose zone is substantially lower than the release concentration (100 mg/L) for PFOS. This is because the majority of the PFOS is adsorbed at the solid–water and air–water interfaces, leaving only a small fraction in the aqueous phase. The second set of simulations—in addition to using K_{aw} at a representative concentration—uses the solution of the full-process numerical model at $t = 30$ years as the initial condition and only focuses on simulating post contamination. Comparisons between the two additional simulations with the original simulations are presented in Fig. 4. The scenario for Accusand and NJ climate is used as an example. The results show that using the representative K_{aw} leads to greater leaching and a better agreement with the full-process numerical model (see the first two rows of Fig. 4). The post-contamination simulation that uses the 30-year solution of the full-process numerical model as the initial condition further improves the prediction of the simplified analytical model. The above results and analysis demonstrate that the deviations observed for PFOS in Figs. 2 and 3 are indeed in part caused by the steady-state infiltration and linear air–water interfacial assumptions employed in the original simulations. Furthermore, the simplified analytical model can be improved by using a representative aqueous concentration to compute K_{aw} , and when simulating post contamination, which would be the case for most of the legacy contamination sites.

We point out that the PFAS contamination scenarios considered here—AFFF-impacted fire training area sites—are among the PFAS source zones with the highest concentrations as demonstrated by many prior field investigations (e.g., Anderson et al., 2019; Brusseau et al., 2020). PFAS concentrations at other source zones including agricultural lands that receive PFAS-contaminated biosolids and irrigation water and wastewater treatment plant sites are often several orders of magnitude lower (e.g., Brusseau et al., 2020). Therefore, it is expected that the linear air–water interfacial adsorption employed in the simplified analytical model would be more appropriate for other source zones compared to the simulations presented here for the AFFF-impacted fire training area sites.

Finally, we note that there is an ongoing debate as to whether the air–water interfacial adsorption can be considered linear at lower concentrations (Schaefer et al., 2019a, 2020; Arshadi et al., 2020), i.e., whether Eq. (9) or another equation that represents Freundlich adsorption should be used to compute the air–water interfacial coefficient. Some additional data and analyses were recently added to this discussion. Brusseau (2021) reported that the air–water interfacial adsorption of two hydrocarbon surfactants (SDS and SDBS) determined by Eq. (9) matches with the air–water interfacial adsorption measured directly by neutron reflectometry for concentrations down to lower than 10^{-5} M. In another study, Brusseau et al. (2021) employed miscible-displacement data of PFOA at a concentration of $C = 1$ μ g/L and showed that the air–water interfacial coefficient computed from the experimental breakthrough curve matches well with that determined by Eq. (9). Nevertheless, further research and data are needed to test the potential nonlinearity of air–water interfacial adsorption at lower concentrations for a wider range of PFAS and under a broader range of conditions.

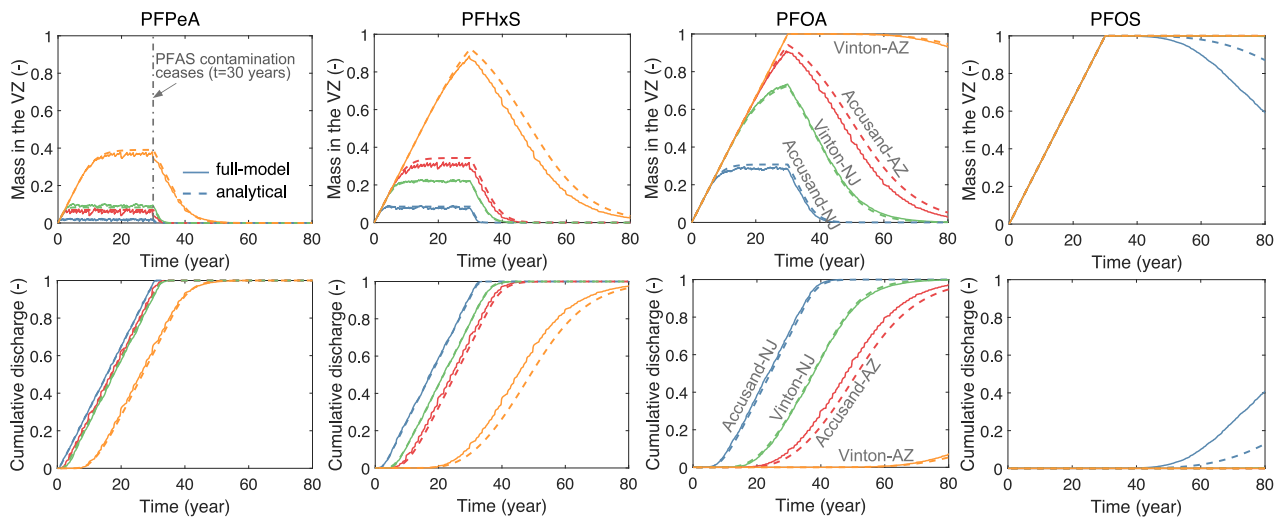


Fig. 2. Comparisons between the simplified analytical model and the full-process numerical model for the simulated PFAS mass retained in the vadose zone (row 1) and the cumulative mass discharge to groundwater (row 2) over time. The four columns correspond to the four PFAS (PFPeA, PFHxS, PFOA, PFOS). Both the mass in the vadose zone and cumulative mass discharge are normalized by the total mass released to the vadose zone during the active-contamination period.

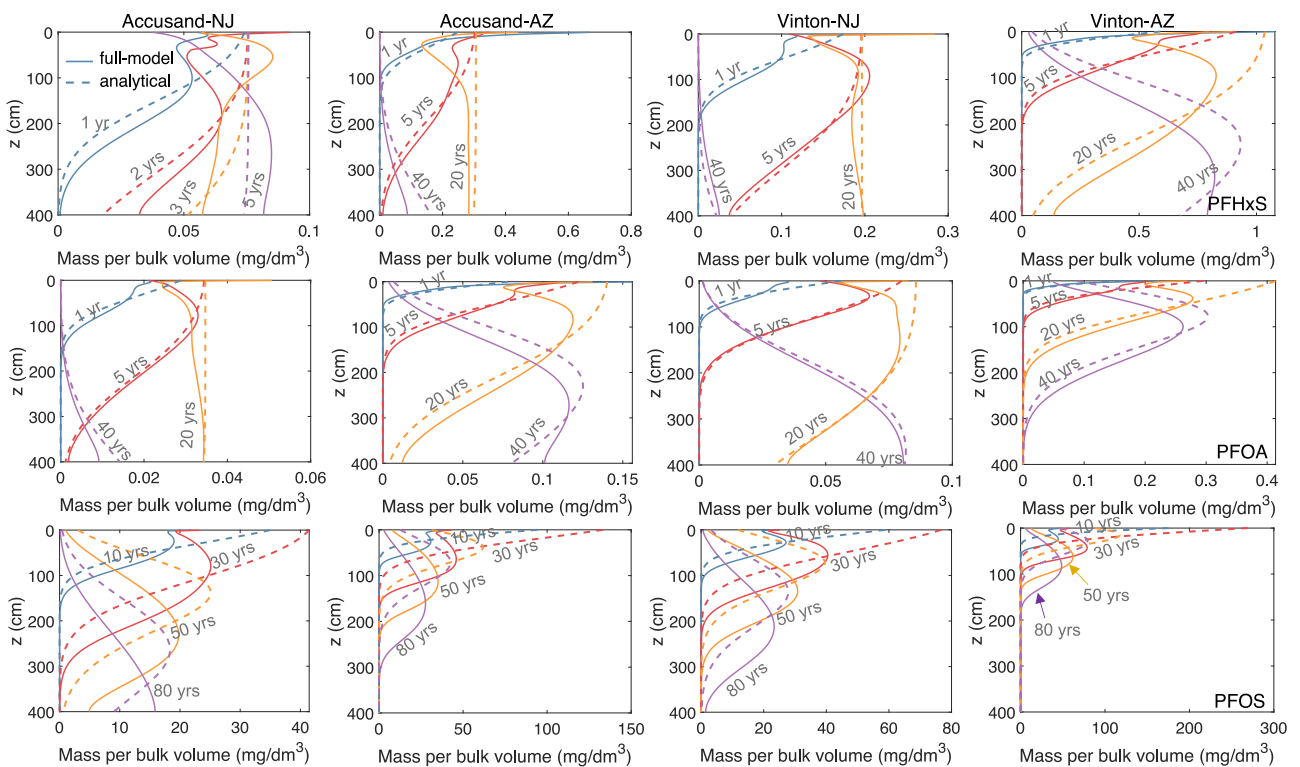


Fig. 3. Comparisons between the simplified analytical model and the full-process numerical model for the simulated time-dependent spatial concentration profiles of PFAS. The mass concentration per bulk volume of soil media represents the combination of PFAS dissolved in the aqueous phase, and adsorbed at the solid-water and air-water interfaces. The three rows correspond to the three PFAS (PFHxS, PFOA, and PFOS). The results for PFPeA are not shown because most of the PFPeA mass is discharged to groundwater shortly after the contamination stops at $t = 30$ years. The four columns denote the four different scenarios, i.e., soil media (Accusand and Vinton soil) and climatic conditions (“AZ” denotes Arizona and “NJ” denotes New Jersey).

5. Demonstration of model application

We present a workflow to demonstrate how to employ the simplified analytical model as a screening tool for analyzing PFAS retention and leaching at field contamination sites. We take a model AFFF-impacted fire training area site as an example for the demonstration. Suppose we are interested in quantifying the leaching of nine representative PFAS varying in headgroups and chain lengths (six PFCAs and three perfluoroalkanesulfonic acids (PFSAs)) in a homogeneous vadose zone

represented by six soils. The annual net water recharge rate is assumed 30 cm. Similar to the scenarios considered in Section 4.2, we consider an active contamination period of 30 years followed by 50 years of post contamination.

For the nine PFAS, the Szyskowski parameters for the surface tension in synthetic groundwater (Silva et al., 2019, 2021), molecular weights, and the release concentrations from a diluted AFFF solution (Høisæter et al., 2019) are provided in Table 2. The six soils include sand (soil 1), sandy loam (soil 2), two loams (soils 3&4),

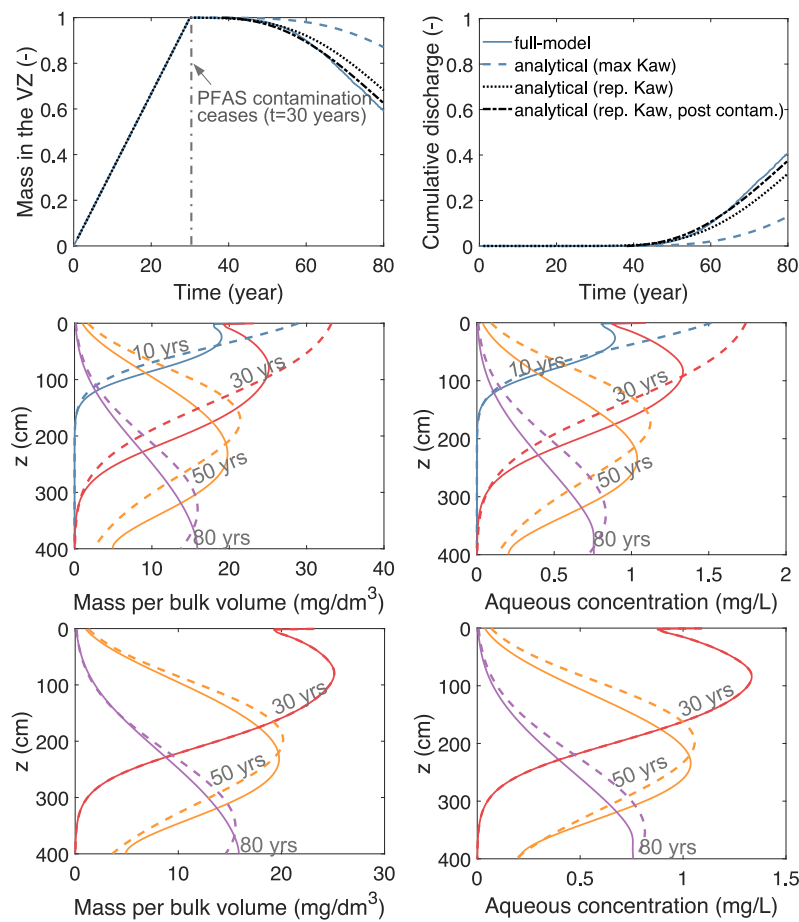


Fig. 4. Simulated long-term retention and leaching of PFOS in the vadose zone using the simplified analytical model with different initial conditions and air–water interfacial adsorption coefficients. The PFOS mass retained in the vadose zone and the cumulative mass discharge to groundwater are shown in the first row, both of which are normalized by the total mass of PFOS released to the vadose zone during the active-contamination period. The spatial profiles of PFOS concentration are presented in the second row (the simulation using K_{aw} at C_{rep}) and third row (the simulation using K_{aw} at C_{rep} and only considers post contamination). The mass concentration per bulk volume of soil media represents the combination of PFOS dissolved in the aqueous phase, and adsorbed at the solid–water and air–water interfaces. All of the simulations are for the scenario of Accusand under NJ climate.

Table 2

Parameters for PFAS including Szyskowski parameters for surface tension, molecular weight, molecular diffusion coefficients, and the release concentrations in the diluted AFFF solution. The surface tension parameters for the PFCAs and PFASs were reported in Silva et al. (2019) and Silva et al. (2021), respectively. The molecular diffusion coefficients were reported in Schaefer et al. (2019b). The PFAS concentrations in the diluted AFFF solution are estimated from a commercial AFFF product reported in Høisæter et al. (2019). Note that the release concentrations need to be converted to C_0 in Eq. (13) assuming steady-state infiltration based on the net recharge rate.

PFAS	a mg/L	b –	M g/mol	D_0 ($\times 10^{-6}$) cm^2/s	Concentration mg/L
PFPeA	3168.6	0.22	264.05	12	0.23
PFHxA	1350.42	0.21	314.05	7.8	0.75
PFHpA	345.86	0.22	364.06	9.3	0.3
PFOA	62.11	0.19	414.07	4.9	0.9
PFNA	5.11	0.16	464.08	2.93	0.0031
PFDA	3.7	0.17	514.08	2.27	0.0015
PFBS	2400.8	0.15	300.1	11	1.4
PFHxS	160.05	0.14	400.12	4.5	7.1
PFOS	3.65	0.12	500.13	5.4	100

sandy clay (soil 5), and a sandy clay loam (soil 6). For the present study, the solid-phase adsorption coefficients for the six soils were measured for the nine PFAS (Nguyen et al., 2020) and are summarized in Table 3. If no measured solid-phase adsorption coefficients are available, they may be estimated using the so-called distributed-sorption models that represent the contribution of individual soil constituents (soil organic carbon, clay minerals, metal oxides) to the total sorption.

Table 3

Solid-phase adsorption coefficients for the nine PFAS in the six soils obtained from Nguyen et al. (2020). The textures for the six soils are sand, sandy loam, two loams, sandy clay, and sandy clay loam, respectively.

PFAS	K_d (cm^3/g)					
	Soil 1	Soil 2	Soil 3	Soil 4	Soil 5	Soil 6
PFPeA	0.04	0.44	0.2	0.15	0.24	0.35
PFHxA	0.05	0.52	0.21	0.17	0.24	0.35
PFHpA	0.3	1.41	0.47	0.46	0.5	0.61
PFOA	0.53	2.84	1.42	0.64	0.81	0.68
PFNA	1.27	10.69	1.77	2	1.31	1.57
PFDA	7.53	45.75	7.96	12.3	16.87	0.86
PFBS	0.05	0.5	0.2	0.17	0.25	0.36
PFHxS	0.28	2.12	0.39	0.45	0.4	0.69
PFOS	3.22	34.3	3.52	4.18	3.15	3.45

The distributed-sorption models can implicitly represent the different potential sorption mechanisms such as hydrophobic and electrostatic interactions and have been developed and applied for quantifying the solid-phase adsorption of PFOA and PFOS in soil media (Higgins and Luthy, 2007; Knight et al., 2019; Wang et al., 2021). The hydraulic parameters for the six soils are not available and are estimated (see Table 4) using the Rosetta pedotransfer model (Zhang and Schaap, 2017) based on soil texture and bulk density reported in Nguyen et al. (2020). No measurements of air–water interfacial area are available for the soils. One approach is to employ the thermodynamic-based method to estimate the air–water interfacial area as a function of

Table 4

Hydraulic and transport parameters for the six soils employed in Section 5. The textures for the six soils are sand, sandy loam, two loams, sandy clay, and sandy clay loam, respectively. The hydraulic parameters including K_s , θ_s , θ_r , α , and n are estimated by the Rosetta pedotransfer model (Zhang and Schaap, 2017) based on soil texture and bulk density reported in Nguyen et al. (2020). The dispersion coefficient α_L is approximated using the empirical model of Xu and Eckstein (1995) where the dependence of α_L on water saturation is not considered.

Soil	K_s cm/day	θ_s cm ³ /cm ³	θ_r cm ³ /cm ³	ρ_b g/cm ³	α cm ⁻¹	n -	α_L cm
Soil 1	482.7	0.363	0.054	1.58	0.03133	2.72	24.39
Soil 2	211.1	0.570	0.097	0.82	0.01291	1.38	24.39
Soil 3	6.1	0.361	0.079	1.59	0.01072	1.362	24.39
Soil 4	10.1	0.384	0.079	1.47	0.00893	1.411	24.39
Soil 5	8.2	0.383	0.111	1.66	0.01364	1.238	24.39
Soil 6	16.2	0.371	0.090	1.59	0.01095	1.327	24.39

water saturation (Leverett, 1941; Morrow, 1970; Bradford and Leij, 1997). The thermodynamic-based method assumes that the mechanical work done for fluid–fluid displacement is fully converted to surface energy (i.e., generating air–water interfaces). As a result, the air–water interfacial area can be estimated by computing the area under the capillary pressure–water saturation curve as

$$A_{aw} = \frac{\phi}{\sigma} \int_{S_w}^1 p_c(S_w) dS_w, \quad (30)$$

where ϕ is the porosity of the soil, σ is the surface tension, and p_c is the capillary pressure. Prior studies have shown that the thermodynamic-based method significantly underestimates the air–water interfacial area compared to that measured by aqueous interfacial tracers (Jiang et al., 2020), but the latter was suggested to be more relevant for PFAS transport in the vadose zone (Brusseau and Guo, 2021). Here, we employ a scaling method to correct the estimated air–water interfacial area estimated from the thermodynamic-based method. We take the Vinton soil introduced in Section 4.2 to compute the ratio between the A_{aw} estimated from the thermodynamic-based method and the measured A_{aw} by aqueous interfacial tracer. The ratio varies from 3.89 to 4.41 for the entire saturation range. As an approximation, the mean ratio 4.15 is applied to correct the air–water interfacial area for the six soils. When computing the thermodynamic-based A_{aw} , the surface tension σ in Eq. (30) is taken as the surface tension with no dissolved PFAS. Note that because parameters for kinetic solid-phase adsorption are not available, kinetic solid-phase adsorption is not accounted for in these simulations.

The simulated PFAS retention in the vadose zone is presented in Fig. 5 for the nine PFAS in the six soils. The results clearly demonstrate that the retention of PFAS vary strongly with different chain lengths and functional groups. For both PFCAs and PFSAs, the longer-chain PFAS are much more strongly retained in the vadose zone than their shorter-chain counterparts, which is consistent with the increasing solid-phase and air–water interfacial adsorption for longer-chain PFAS. While variations in the retention of a given PFAS exist among the six soils, the difference between the soils is not significant except for soil 2, which has the strongest retention due to its much stronger solid-phase adsorption. The similar retention among the soils is in part caused by the same net recharge rate (30 cm per year) employed for all of the six soils. At field sites, the net recharge rate will likely change with different soils in the vadose zone as a result of different surface evaporation rates due to different water retention capacities. For example, this was the case for the Accusand and Vinton soil employed in Section 4.2, where their net recharge rates differ by almost 2 times. This also implies that it is critical to obtain a more accurate estimate of the net recharge rate for improved prediction of PFAS retention and leaching in the vadose zone when applying the simplified analytical model.

Another way to analyze the strength of retention is to compare the retardation factors among different PFAS and soils. The computed retardation factors are presented in Fig. 6, from which we can make the

following observations. Consistent with the retention behavior shown in Fig. 5, the retardation factors increase with chain length for the same soil. The retardation factors for the short-chain PFAS (PFPeA, PFHxA, PFHpA, and PFBS) are smaller than 10 for all soils except for PFHpA in soil 1 (sand) that has a retardation factor of 11.1. Comparisons among the soils reveal that for the longer-chain PFAS, the retardation factors for soil 1 (sand) and soil 2 (sandy loam) are greater than the other finer-grain soils. The reason for this rather counterintuitive observation is that, for a given infiltration rate, the finer-grain soils have a much higher water saturation that leads to a much smaller air–water interfacial area. This then leads to reduced air–water interfacial adsorption and total retention of PFAS in the vadose zone comprised of finer-grain soils. Overall, the above workflow and analyses demonstrate that the simplified analytical model provides a computationally efficient means to quantify PFAS leaching in the vadose zone and mass discharge to groundwater.

6. Summary and conclusion

We present a simplified model for quantifying PFAS leaching in the vadose zone and mass discharge to groundwater. The model assumes steady-state infiltration and linear solid-phase and air–water interfacial adsorption. Rate-limited solid-phase adsorption is represented by a two-domain kinetic model. Air–water interfacial adsorption is assumed instantaneous (i.e., equilibrium). New analytical solutions for the simplified model are derived that allow for arbitrary initial conditions. These analytical solutions are the first that account for the two-domain solid-phase kinetic adsorption and air–water interfacial adsorption for solute transport. While the model formulation involves a number of simplifications, predicted simulations using the analytical solution agree well with a wide range of sand-packed miscible-displacement experiments for PFAS under water-unsaturated conditions. For these experiments, the analytical solution is almost identical to the solution from a numerical model that accounts for a set of comprehensive PFAS-specific transport processes, including surfactant-induced flow and rate-limited and nonlinear adsorption at the solid–water and air–water interfaces. These comparisons demonstrate the validity of the simplified model and the analytical solution for representing the PFAS-specific transport processes under laboratory conditions. The simplified model is then compared to the full-process numerical model for simulating long-term PFAS leaching at a model AFFF-impacted fire training area site. Despite that several processes and conditions are not represented in the simplified model, e.g., surfactant-induced flow, time-dependent infiltration and evapotranspiration, and nonlinearity in the solid–water and air–water interfacial adsorption, close agreement is observed between the simplified analytical and full-process numerical models in their simulated long-term retention of PFAS in the vadose zone and mass discharge to groundwater.

Practically, the analytical solution provides a simple approach for estimating PFAS retention and leaching in the vadose zone and mass discharge to groundwater at PFAS-contamination sites. This screening-type tool allows stakeholders and practitioners to develop quantitative guidance for characterizing, managing, and mitigating the long-term risks of PFAS contamination. In particular, because the simplified model can be solved analytically, 1,000s of simulations can be easily conducted for a given problem using a wide range of input parameters. These simulations can be used to quantify the uncertainty propagated from the input parameters to the final predictions and also to gain critical insights into the primary parameters or factors that control the long-term risks of PFAS contamination at sites. In addition to the computationally-focused analyses, this screening-type tool can also be combined with direct measurements of soil porewater concentrations proposed in a recent perspective by Anderson (2021) for quantifying soil-to-groundwater mass discharge and providing remedial guidance at PFAS-contamination sites.

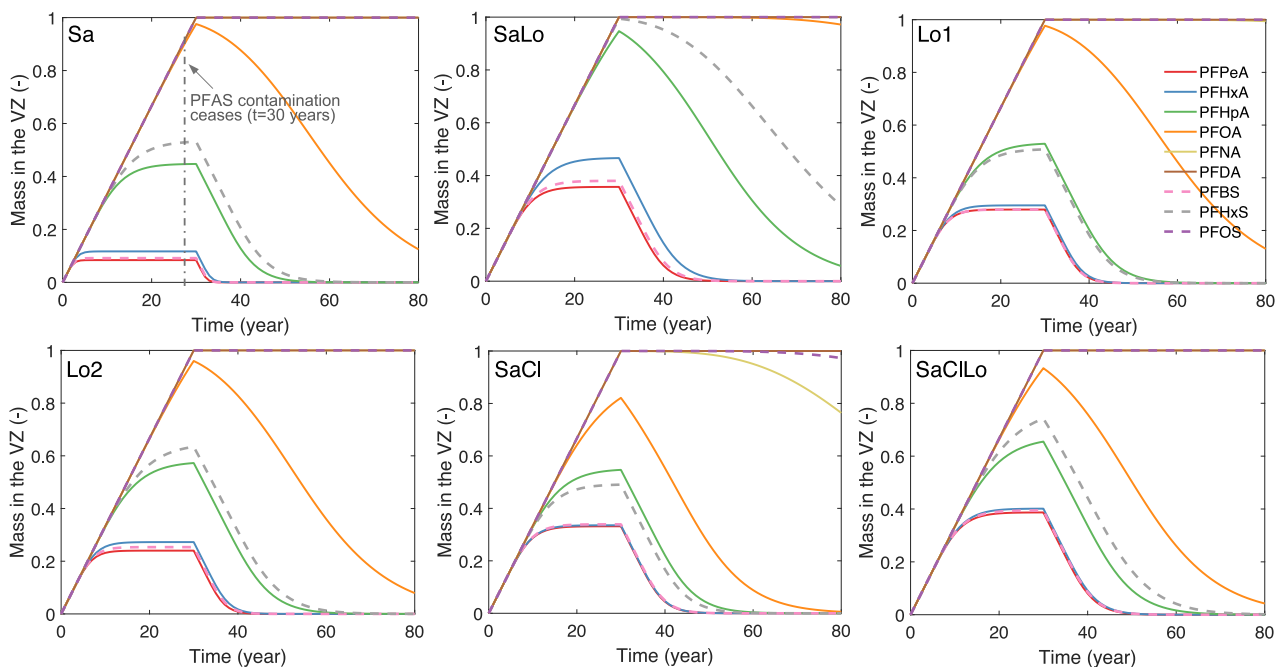


Fig. 5. Simulated retention of nine PFAS (six PFCAs and three PFSA) in a homogeneous vadose zone represented by six soils. The soil textures are: sand (Sa), sandy loam (SaLo), two loams (Lo1 and Lo2), sandy clay (SaCl), and sandy clay loam (SaClLo). The solid and dashed lines denote PFCAs and PFSA, respectively.

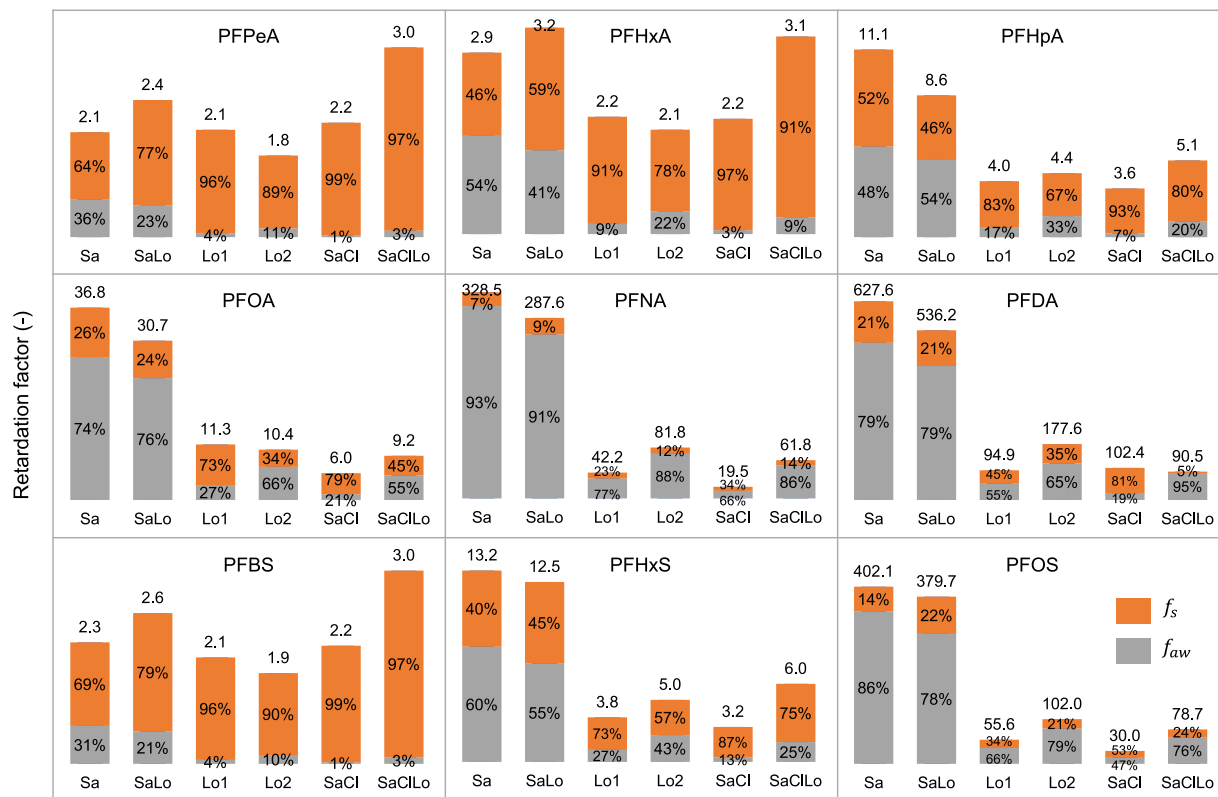


Fig. 6. Simulated retardation factors for the nine PFAS in a homogeneous vadose zone represented by six soils. The soil textures are: sand (Sa), sandy loam (SaLo), two loams (Lo1 and Lo2), sandy clay (SaCl), and sandy clay loam (SaClLo). The number at the top of each bar is the total retardation factor R . The orange and gray portions of the bar denote, respectively, the fraction contributed by solid-phase adsorption ($f_s = R_s / (R - 1)$) and the fraction contributed by air-water interfacial adsorption ($f_{aw} = R_{aw} / (R - 1)$). (For interpretation of the references to color in this figure legend, the reader is referred to the web version of this article.)

The simplified model is nevertheless limited by the imposed assumptions. Here, we briefly discuss the limitations and propose strategies that may be employed to partially address these limitations when applying the model to analyze practical problems. For example, the

analytical solution is unable to simulate PFAS leaching in the presence of spatial heterogeneities such as soil layering that can lead to both heterogeneous hydraulic and sorption properties (Zeng and Guo, 2021). The impact of heterogeneities may be indirectly accounted for by

conducting a range of simulations using different soil types relevant to a specific site. These simulations can be used to provide upper and lower bounds for the estimates of PFAS leaching and mass discharge. Similarly, since the analytical solution is derived under steady-state infiltration, it cannot represent the impact of dynamic infiltration on PFAS leaching. However, the simulation results presented in Section 4.2 show that the simulated PFAS leaching by assuming steady-state flow agrees well with those generated by the full-process numerical model that accounts for highly dynamic infiltration rates from real rainfall data at a 30-min temporal resolution. While only homogeneous vadose zones are considered in Section 4.2, a prior study by Russo and Fiori (2008) suggested that assuming steady-state flow is sufficient for predicting solute transport even in heterogeneous vadose zones (note that a non-surfactant solute in the absence of complex retention processes was considered therein), provided that the groundwater table is located at sufficiently large distance from the land surface. Nonetheless, when dynamic infiltration does influence PFAS leaching, as a practical approach, one may examine the impact of varying infiltration rates by comparing results from a range of simulations that cover the common or possible ranges in infiltration rates.

CRedit authorship contribution statement

Bo Guo: Conceptualization, Methodology, Investigation, Software, Data curation, Formal analysis, Visualization, Writing – original draft. **Jicai Zeng:** Data curation, Visualization, Writing – review & editing. **Mark L. Brusseau:** Data curation, Formal analysis, Writing – review & editing. **Yonggen Zhang:** Data curation, Writing – review & editing.

Declaration of competing interest

The authors declare that they have no known competing financial interests or personal relationships that could have appeared to influence the work reported in this paper.

Acknowledgment

This work was supported by the Environmental Security Technology Certification Program, United States (Project ER21-5041), the National Science Foundation, United States (2023351), and the Superfund Research Program of the NIEHS (P42 ES4940). The analytical solutions presented in this paper have been implemented into a computer code that is available from the corresponding author upon reasonable request.

Appendix. Special case of the analytical solution (equilibrium adsorption)

When the solid-phase adsorption can be assumed equilibrium, i.e., $F_s = 1$ and $C_{s,2} = 0$, Eq. (10) reduces to the standard advection-dispersion equation with a constant retardation factor representing the combined retention from equilibrium solid-water and air-water interfacial adsorption. Here, we present the analytical solution for this special case. The solution for the boundary value problem is available in the literature as summarized in van Genuchten and Alves (1982)

$$C^{BVP}(Z, T) = \begin{cases} C_0 A(Z, T), & 0 < T \leq T_0 \\ C_0 A(Z, T) - C_0 A(Z, T - T_0), & T > T_0 \end{cases} \quad (31)$$

where $A(Z, T) = \frac{1}{2} \operatorname{erfc} \left[\frac{RZ - T}{2(TR/P)^{1/2}} \right] + \left(\frac{TP}{\pi R} \right)^{1/2} e^{-\frac{(RZ - T)^2}{4TR/P}} - \frac{1}{2} (1 + PZ + \frac{PT}{R}) e^{PZ} \operatorname{erfc} \left(\frac{RZ + T}{2(TR/P)^{1/2}} \right)$.

The solution for the initial value problem with an arbitrary initial condition has the following form (Lindstrom and Narasimham, 1973)

$$C^{IVP}(Z, T) = \int_0^\infty C_i(\xi)$$

$$\left[\frac{e^{-(RZ - R\xi - T)^2 / (4TR/P)} + e^{(-P\xi - (RZ + R\xi - T)^2 / (4TR/P)) / (2\sqrt{\pi T / (PR)})}}{2\sqrt{\pi T / (PR)}} - \frac{P}{2} e^{PZ} \operatorname{erfc} \left(\frac{RZ + R\xi + T}{2\sqrt{TR/P}} \right) \right] d\xi. \quad (32)$$

$C(Z, T) = C^{BVP}(Z, T) + C^{IVP}(Z, T)$ then gives the full solution for this special case with equilibrium solid-water and air-water interfacial adsorption.

References

Adamson, A.W., Gast, A.P., 1997. *Physical Chemistry of Surfaces*. John Wiley & Sons, Inc, New York.

Adamson, D.T., Nickerson, A., Kulkarni, P.R., Higgins, C.P., Popovic, J., Field, J., Rodowa, A., Newell, C., DeBlanc, P., Kornuc, J.J., 2020. Mass-based, field-scale demonstration of PFAS retention within AFFF-associated source areas. *Environ. Sci. Technol.* 54, 15768–15777.

Anderson, R.H., 2021. The case for direct measures of soil-to-groundwater contaminant mass discharge at AFFF-impacted sites. *Environ. Sci. Technol.* 55, 6580–6583.

Anderson, R.H., Adamson, D.T., Stroo, H.F., 2019. Partitioning of poly-and perfluoroalkyl substances from soil to groundwater within aqueous film-forming foam source zones. *J. Contam. Hydrol.* 220, 59–65.

Arshadi, M., Costanza, J., Abriola, L.M., Pennell, K.D., 2020. Comment on Uptake of poly-and perfluoroalkyl substances at the air–water interface. *Environ. Sci. Technol.* 54, 7019–7020.

Barzen-Hanson, K.A., Davis, S.E., Kleber, M., Field, J.A., 2017. Sorption of fluorotelomer sulfonates, fluorotelomer sulfonamido betaines, and a fluorotelomer sulfonamido amine in national foam aqueous film-forming foam to soil. *Environ. Sci. Technol.* 51, 12394–12404.

Bradford, S.A., Leij, F.J., 1997. Estimating interfacial areas for multi-fluid soil systems. *J. Contam. Hydrol.* 27, 83–105.

Brusseau, M.L., 2018. Assessing the potential contributions of additional retention processes to PFAS retardation in the subsurface. *Sci. Total Environ.* 613, 176–185.

Brusseau, M.L., 2019. The influence of molecular structure on the adsorption of PFAS to fluid-fluid interfaces: Using QSPR to predict interfacial adsorption coefficients. *Water Res.* 152, 148–158.

Brusseau, M.L., 2020. Simulating PFAS transport influenced by rate-limited multi-process retention. *Water Res.* 168, 115179.

Brusseau, M.L., 2021. Examining the robustness and concentration dependency of PFAS air–water and NAPL-water interfacial adsorption coefficients. *Water Res.* 190, 116778.

Brusseau, M.L., Anderson, R.H., Guo, B., 2020. PFAS concentrations in soils: Background levels versus contaminated sites. *Sci. Total Environ.* 740, 140017.

Brusseau, M.L., Guo, B., 2021. Air-water interfacial areas relevant for transport of per and poly-fluoroalkyl substances. *Water Res.* 117785.

Brusseau, M.L., Guo, B., Huang, D., Yan, N., Lyu, Y., 2021. Ideal versus nonideal transport of PFAS in unsaturated porous media. *Water Res.* 117405.

Brusseau, M.L., Khan, N., Wang, Y., Yan, N., van Glubt, S., Carroll, K.C., 2019a. Nonideal transport and extended elution tailing of PFOS in soil. *Environ. Sci. Technol.*

Brusseau, M.L., Van Glubt, S., 2021. The influence of molecular structure on PFAS adsorption at air–water interfaces in electrolyte solutions. *Chemosphere* 281, 130829.

Brusseau, M.L., Yan, N., Van Glubt, S., Wang, Y., Chen, W., Lyu, Y., Dungan, B., Carroll, K.C., Holguin, F.O., 2019b. Comprehensive retention model for PFAS transport in subsurface systems. *Water Res.* 148, 41–50.

Cáñez, T.T., Guo, B., McIntosh, J.C., Brusseau, M.L., 2021. Perfluoroalkyl and polyfluoroalkyl substances (PFAS) in groundwater at a reclaimed water recharge facility. *Sci. Total Environ.* 147906.

Chang, C.-H., Franses, E.I., 1995. Adsorption dynamics of surfactants at the air/water interface: a critical review of mathematical models, data, and mechanisms. *Colloids Surf. A* 100, 1–45.

Costanza, J., Abriola, L.M., Pennell, K.D., 2020. Aqueous film-forming foams exhibit greater interfacial activity than PFOA, PFOS, or FOSA. *Environ. Sci. Technol.* 54, 13590–13597.

Costanza, J., Arshadi, M., Abriola, L.M., Pennell, K.D., 2019. Accumulation of PFOA and PFOS at the air–water interface. *Environ. Sci. Technol. Lett.* 6, 487–491.

Dauchy, X., Boiteux, V., Colin, A., Hémard, J., Bach, C., Rosin, C., Munoz, J.-F., 2019. Deep seepage of per- and polyfluoroalkyl substances through the soil of a firefighter training site and subsequent groundwater contamination. *Chemosphere* 214, 729–737.

El Ouni, A., Guo, B., Zhong, H., Brusseau, M.L., 2021. Testing the validity of the miscible-displacement interfacial tracer method for measuring air–water interfacial area: Independent benchmarking and mathematical modeling. *Chemosphere* 263, 128193.

- Falta, R., Farhat, S., Newell, C., Lynch, K., 2018. REMChlor-MD, Developed for the Environmental Security Technology Certification Program (ESTCP) by Clemson University, Clemson. South Carolina and GSI Environmental Inc., Houston, Texas, URL: <https://www.gsi-net.com/en/software/free-software/remchlormd.html>.
- van Genuchten, M.T., 1980. A closed-form equation for predicting the hydraulic conductivity of unsaturated soils 1. *Soil Sci. Am. J.* 44, 892–898.
- van Genuchten, M.T., 1981. Non-Equilibrium Transport Parameters from Miscible Displacement Experiments. US Dept. of Agriculture, Science and Education Administration, US Salinity.
- van Genuchten, M.T., Alves, W., 1982. Analytical Solutions of the One-Dimensional Convective-Dispersive Solute Transport Equation. Dept. of Agriculture. Technical bulletin (USA), United States.
- van Genuchten, M.T., Parker, J., 1984. Boundary conditions for displacement experiments through short laboratory soil columns. *Soil Sci. Am. J.* 48, 703–708.
- van Genuchten, M.T., Wagenet, R., 1989. Two-site/two-region models for pesticide transport and degradation: Theoretical development and analytical solutions. *Soil Sci. Am. J.* 53, 1303–1310.
- Guelfo, J.L., Higgins, C.P., 2013. Subsurface transport potential of perfluoroalkyl acids at aqueous film-forming foam (AFFF)-impacted sites. *Environ. Sci. Technol.* 47, 4164–4171.
- Guelfo, J.L., Wunsch, A., McCray, J., Stults, J.F., Higgins, C.P., 2020. Subsurface transport potential of perfluoroalkyl acids (PFAAs): Column experiments and modeling. *J. Contam. Hydrol.* 233, 103661.
- Guo, B., Zeng, J., Brusseau, M.L., 2020. A mathematical model for the release, transport, and retention of per-and polyfluoroalkyl substances (PFAS) in the vadose zone. *Water Resour. Res.* 56, e2019WR026667.
- Higgins, C.P., Luthy, R.G., 2006. Sorption of perfluorinated surfactants on sediments. *Environ. Sci. Technol.* 40, 7251–7256.
- Higgins, C.P., Luthy, R.G., 2007. Modeling sorption of anionic surfactants onto sediment materials: an a priori approach for perfluoroalkyl surfactants and linear alkylbenzene sulfonates. *Environ. Sci. Technol.* 41, 3254–3261.
- Høisæter, Å., Pfaff, A., Breedveld, G.D., 2019. Leaching and transport of PFAS from aqueous film-forming foam (AFFF) in the unsaturated soil at a firefighting training facility under cold climatic conditions. *J. Contam. Hydrol.* 222, 112–122.
- Houtz, E.F., Higgins, C.P., Field, J.A., Sedlak, D.L., 2013. Persistence of perfluoroalkyl acid precursors in AFFF-impacted groundwater and soil. *Environ. Sci. Technol.* 47, 8187–8195.
- Jiang, H., Guo, B., Brusseau, M.L., 2020. Pore-scale modeling of fluid-fluid interfacial area in variably saturated porous media containing microscale surface roughness. *Water Resour. Res.* 56, e2019WR025876.
- Kissa, E., 2001. Fluorinated Surfactants and Repellents, Vol. 97. CRC Press.
- Knight, E.R., Janik, L.J., Navarro, D.A., Kookana, R.S., McLaughlin, M.J., 2019. Predicting partitioning of radiolabelled 14C-PFOA in a range of soils using diffuse reflectance infrared spectroscopy. *Sci. Total Environ.* 686, 505–513.
- Kosugi, K., 1999. General model for unsaturated hydraulic conductivity for soils with lognormal pore-size distribution. *Soil Sci. Am. J.* 63, 270–277.
- Kreft, A., Zuber, A., 1978. On the physical meaning of the dispersion equation and its solutions for different initial and boundary conditions. *Chem. Eng. Sci.* 33, 1471–1480.
- Leverett, M., 1941. Capillary behavior in porous solids. *Trans. AIME* 142, 152–169.
- Li, Z., Lyu, X., Gao, B., Xu, H., Wu, J., Sun, Y., 2021. Effects of ionic strength and cation type on the transport of perfluoroctanoic acid (PFOA) in unsaturated sand porous media. *J. Hard Mater.* 403, 123688.
- Lindstrom, F., Narasimham, M., 1973. Mathematical theory of a kinetic model for dispersion of previously distributed chemicals in a sorbing porous medium. *SIAM J. Appl. Math.* 24, 496–510.
- Lindstrom, F., Stone, W., 1974. On the start up or initial phase of linear mass transport of chemicals in a water saturated sorbing porous medium. I. *SIAM J. Appl. Math.* 26, 578–591.
- Lyu, Y., Brusseau, M.L., Chen, W., Yan, N., Fu, X., Lin, X., 2018. Adsorption of PFOA at the air–water interface during transport in unsaturated porous media. *Environ. Sci. Technol.* 52, 7745–7753.
- Lyu, X., Liu, X., Sun, Y., Gao, B., Ji, R., Wu, J., Xue, Y., 2020. Importance of surface roughness on perfluoroctanoic acid (PFOA) transport in unsaturated porous media. *Environ. Pollut.* 266, 115343.
- Mejia-Avenidaño, S., Zhi, Y., Yan, B., Liu, J., 2020. Sorption of polyfluoroalkyl surfactants on surface soils: Effect of molecular structures, soil properties, and solution chemistry. *Environ. Sci. Technol.* 54, 1513–1521.
- Millington, R., Quirk, J., 1961. Permeability of porous solids. *Trans. Faraday Soc.* 57, 1200–1207.
- Morrow, N.R., 1970. Physics and thermodynamics of capillary action in porous media. *Ind. Eng. Chem.* 62, 32–56.
- Mualem, Y., 1976. A new model for predicting the hydraulic conductivity of unsaturated porous media. *Water Resour. Res.* 12, 513–522.
- Nguyen, T.M.H., Braunig, J., Thompson, K., Thompson, J., Kabiri, S., Navarro, D.A., Kookana, R.S., Grimison, C., Barnes, C.M., Higgins, C.P., et al., 2020. Influences of chemical properties, soil properties, and solution pH on soil–water partitioning coefficients of per-and polyfluoroalkyl substances (PFASs). *Environ. Sci. Technol.* 54, 15883–15892.
- Rosen, M.J., Kunjappu, J.T., 2012. Surfactants and Interfacial Phenomena. John Wiley & Sons.
- Russo, D., Fiori, A., 2008. Equivalent vadose zone steady state flow: An assessment of its capability to predict transport in a realistic combined vadose zone–groundwater flow system. *Water Resour. Res.* 44.
- Schaefer, C.E., Culina, V., Nguyen, D., Field, J., 2019a. Uptake of poly-and perfluoroalkyl substances at the air–water interface. *Environ. Sci. Technol.* 53, 12442–12448.
- Schaefer, C.E., Drennan, D.M., Tran, D.N., Garcia, R., Christie, E., Higgins, C.P., Field, J.A., 2019b. Measurement of aqueous diffusivities for perfluoroalkyl acids. *J. Environ. Eng.* 145, 06019006.
- Schaefer, C.E., Nguyen, D., Christie, E., Shea, S., Higgins, C.P., Field, J.A., 2021. Desorption of poly- and perfluoroalkyl substances from soil historically impacted with aqueous film-forming foam. *J. Environ. Eng.* 147, 06020006.
- Schaefer, C.E., Nguyen, D., Field, J., 2020. Response to the comment on Uptake of poly-and perfluoroalkyl substances at the air–water interface. *Environ. Sci. Technol.* 54, 7021–7022.
- Sharifan, H., Bagheri, M., Wang, D., Burken, J.G., Higgins, C.P., Liang, Y., Liu, J., Schaefer, C.E., Blotvogel, J., 2021. Fate and transport of per-and polyfluoroalkyl substances (PFASs) in the vadose zone. *Sci. Total Environ.* 145427.
- Silva, J.A., Martin, W.A., Johnson, J.L., McCray, J.E., 2019. Evaluating air–water and NAPL-water interfacial adsorption and retention of perfluorocarboxylic acids within the vadose zone. *J. Contam. Hydrol.* 223, 103472.
- Silva, J.A., Martin, W.A., McCray, J.E., 2021. Air–water interfacial adsorption coefficients for PFAS when present as a multi-component mixture. *J. Contam. Hydrol.* 236, 103731.
- Silva, J.A.K., Simunek, J., McCray, J.E., 2020. A modified HYDRUS model for simulating PFAS transport in the vadose zone. *Water* 12, 2758.
- Sima, M.W., Jaffé, P.R., 2020. A critical review of modeling poly- and perfluoroalkyl substances (PFAS) in the soil–water environment. *Sci. Total Environ.* 143793.
- Toride, N., Leij, F.J., van Genuchten, M.T., 1993. A comprehensive set of analytical solutions for nonequilibrium solute transport with first-order decay and zero-order production. *Water Resour. Res.* 29, 2167–2182.
- Umeh, A.C., Naidu, R., Shilpi, S., Boateng, E.B., Rahman, A., Cousins, I.T., Chadalavada, S., Lamb, D., Bowman, M., 2021. Sorption of pfas in 114 well-characterized tropical and temperate soils: Application of multivariate and artificial neural network analyses. *Environ. Sci. Technol.* 55, 1779–1789.
- US-EPA, 2017. EPA Spreadsheet for Modeling Subsurface Vapor Intrusion. URL: <https://www.epa.gov/vaporintrusion/epa-spreadsheet-modeling-subsurface-vapor-intrusion#model>.
- Van Glubt, S., Brusseau, M.L., Yan, N., Huang, D., Khan, N., Carroll, K.C., 2020. Column versus batch methods for measuring PFOS and PFOA sorption to geomeia. *Environ. Pollut.* 268, 115917.
- Wang, Y., Khan, N., Huang, D., Carroll, K.C., Brusseau, M.L., 2021. Transport of PFOS in aquifer sediment: Transport behavior and a distributed-sorption model. *Sci. Total Environ.* 779, 146444.
- Weber, A.K., Barber, L.B., LeBlanc, D.R., Sunderland, E.M., Vecitis, C.D., 2017. Geochemical and hydrologic factors controlling subsurface transport of poly-and perfluoroalkyl substances, Cape Cod, Massachusetts. *Environ. Sci. Technol.* 51, 4269–4279.
- Wei, C., Song, X., Wang, Q., Hu, Z., 2017. Sorption kinetics, isotherms and mechanisms of PFOS on soils with different physicochemical properties. *Ecotoxicol. Environ. Saf.* 142, 40–50.
- Xiao, F., Jin, B., Golovko, S.A., Golovko, M.Y., Xing, B., 2019. Sorption and desorption mechanisms of cationic and zwitterionic per-and polyfluoroalkyl substances in natural soils: thermodynamics and hysteresis. *Environ. Sci. Technol.* 53, 11818–11827.
- Xiao, F., Simcik, M.F., Halbach, T.R., Gulliver, J.S., 2015. Perfluorooctane sulfonate (PFOS) and perfluorooctanoate (PFOA) in soils and groundwater of a US metropolitan area: migration and implications for human exposure. *Water Res.* 72, 64–74.
- Xu, M., Eckstein, Y., 1995. Use of weighted least-squares method in evaluation of the relationship between dispersivity and field scale. *Groundwater* 33, 905–908.
- Yan, N., Ji, Y., Zhang, B., Zheng, X., Brusseau, M.L., 2020. Transport of GenX in saturated and unsaturated porous media. *Environ. Sci. Technol.* 54, 11876–11885.
- Zeng, J., Brusseau, M.L., Guo, B., 2021. Model validation and analyses of parameter sensitivity and uncertainty for modeling long-term retention and leaching of PFAS in the vadose zone. *J. Hydrol.* 127172.
- Zeng, J., Guo, B., 2021. Multidimensional simulation of PFAS transport and leaching in the vadose zone: Impact of surfactant-induced flow and subsurface heterogeneities. *Adv. Water Resour.* 155, 104015.
- Zhang, Y., Schaap, M.G., 2017. Weighted recalibration of the Rosetta pedotransfer model with improved estimates of hydraulic parameter distributions and summary statistics (Rosetta3). *J. Hydrol.* 547, 39–53.
- Zhou, D., Brusseau, M.L., Zhang, Y., Li, S., Wei, W., Sun, H., Zheng, C., 2021. Simulating PFAS adsorption kinetics, adsorption isotherms, and nonideal transport in saturated soil with tempered one-sided stable density (TOSD) based models. *J. Hard Mater.* 411, 125169.